

JGR Earth Surface

L

RESEARCH ARTICLE

10.1029/2024JF008193

Key Points:

- Drone-based video and machine learning tracked 36,000 wood detections during a controlled flood in a Swiss alpine river
- Log transport dynamics were influenced by flow velocity, shape, and size, with large logs contributing 65% of the total volume
- The study bridges lab experiments and field observations, offering tools to advance flood risk assessment and river management

Supporting Information:

Supporting Information may be found in the online version of this article.

Correspondence to:

J. Aarnink, janbert.aarnink@unil.ch

Citation:

Aarnink, J., Fornari, A., Rouge, F., Ceriotti, G., & Ruiz-Villanueva, V. (2025). Tracking floating wood during a flood: New insights from drone surveys and machine learning. *Journal of Geophysical Research: Earth Surface*, *130*, e2024JF008193. https://doi.org/10.1029/ 2024JF008193

Received 29 NOV 2024 Accepted 12 AUG 2025

Author Contributions:

Conceptualization: J. Aarnink Data curation: J. Aarnink, A. Fornari, F. Rouge Formal analysis: J. Aarnink, G. Ceriotti Funding acquisition: V. Ruiz-Villanueva Investigation: J. Aarnink Methodology: J. Aarnink, G. Ceriotti,

V. Ruiz-Villanueva **Project administration:** V. Ruiz-Villanueva

Resources: V. Ruiz-Villanueva Software: J. Aarnink Supervision: V. Ruiz-Villanueva Validation: J. Aarnink Visualization: J. Aarnink

© 2025. The Author(s).

This is an open access article under the terms of the Creative Commons

Attribution License, which permits use, distribution and reproduction in any medium, provided the original work is properly cited.

Tracking Floating Wood During a Flood: New Insights From Drone Surveys and Machine Learning

J. Aarnink¹, A. Fornari¹, F. Rouge¹, G. Ceriotti¹, and V. Ruiz-Villanueva^{1,2}

¹Université de Lausanne, Quartier UNIL-Mouline—Bâtiment Géopolis, Lausanne, Switzerland, ²Geomorphology, Natural Hazards and Risks Unit, Institute of Geography, University of Bern, Bern, Switzerland

Abstract Instream large wood (LW) plays a vital role in river morphology and ecology, but its transport can pose risks to infrastructure during floods. Monitoring LW transport during flood events remains limited due to technical and logistical limitations. This study employs drone-based video monitoring and machine learning to analyze LW dynamics during an experimental flood in the Spöl River, Swiss Alps. Using three drones covering a 200-m stretch, we created a high-resolution data set of over 560 pieces and 36,000 wood detections (including individual pieces captured in multiple frames). Convolutional neural networks (CNNs) detected and tracked LW, enabling detailed analysis of trajectories, rotation, and velocity, complemented with flow field characteristics (i.e., surface velocity) derived from Large-Scale Particle Image Velocimetry (LSPIV). Results showed that LW transport was concentrated in high-velocity flow paths and influenced by wood piece dimensions. Longer, thinner pieces moved faster, while thicker pieces faced greater resistance. Flow convergence aligned wood pieces with flow direction, reducing rotation, especially for larger pieces. Although wood piece rotation increased with flow velocity, it plateaued at the highest velocities. Large pieces, while fewer, represented 65% of the total transported volume, emphasizing their role in LW dynamics. By leveraging unmanned aerial vehicles (UAVs) and convolutional neural networks (CNNs), this study offers new insights into interactions between flow conditions, wood size, and transport behavior. Our findings contribute to the understanding of LW dynamics in flood conditions and provide valuable information that can enhance flood risk assessment, support early warning systems, and inform sustainable river management strategies.

Plain Language Summary This study uses drones and machine learning to investigate the movement of large wood (LW) during a controlled flood in the Spöl River, Swiss Alps. Large wood, including logs and branches, plays a crucial role in shaping river ecosystems but can pose risks during floods. By combining drone video monitoring with advanced neural networks, the research team tracked wood movements along a 200-m stretch. Key findings highlight that larger logs, despite being fewer in number, contributed 65% of the total transported volume due to their size. Log movement was seen after an increase in water level and was influenced by flow velocity and log shape; thinner logs moved faster. Flow convergence aligned logs with the current, reducing rotation, particularly for larger pieces. The study bridges the gap between controlled experiments and real-world observations, offering insights into how log dimensions and flow conditions affect transport dynamics. It emphasizes the value of using drones and AI to improve flood risk assessment and river management strategies. This research enhances understanding of LW behavior during floods and demonstrates the potential of innovative technologies in environmental monitoring and management.

1. Introduction

Instream large wood (LW), defined as logs, root wads, trunks, and branches with a diameter of at least 10 cm and a length of 1 m (Wohl et al., 2010), plays an important role in shaping the dynamics of river ecosystems. Natural processes such as landslides, debris flows, and bank erosion drive LW recruitment in forested watersheds (Hassan et al., 2016; Platts et al., 1987). Once in the river, these individual pieces can form wood jams, eventually trapping sediment and creating heterogeneous channel morphologies with steps, pools, bars, and secondary channels (Andreoli et al., 2007; Gurnell et al., 2002; May & Gresswell, 2003; Wohl et al., 2018). This interplay of LW and sediment enhances habitat complexity, providing valuable feeding grounds for aquatic and terrestrial species (Chen et al., 2008).

On the other hand, during floods, the transport of instream wood may pose hazards and risks (Rickenmann & Koschni, 2010). The transported pieces of LW can get trapped at bridges or other infrastructure and cause a

AARNINK ET AL. 1 of 21



Journal of Geophysical Research: Earth Surface

10.1029/2024JF008193

Writing – original draft: J. Aarnink, G. Ceriotti, V. Ruiz-Villanueva

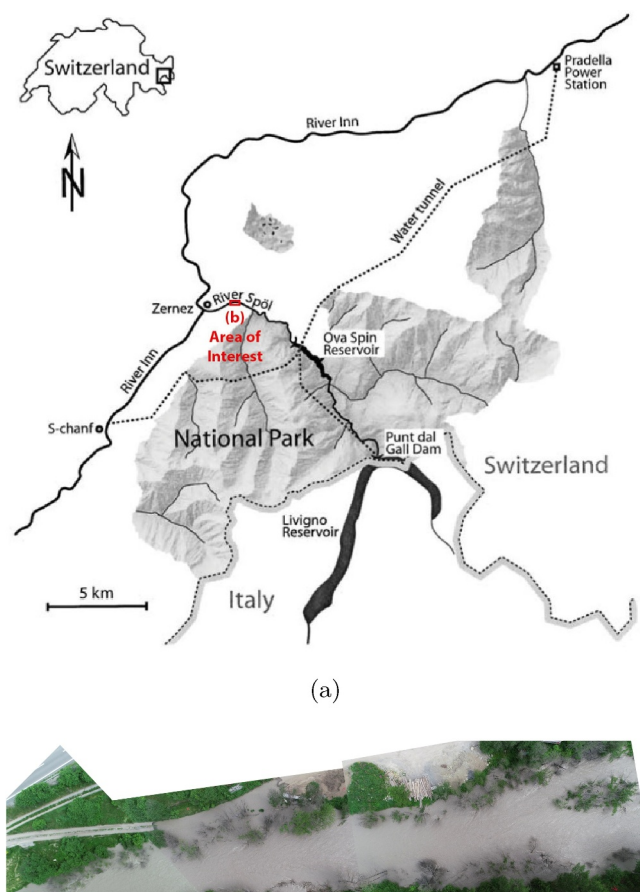
channel blockage, potentially resulting in a backwater rise and larger inundations (Ruiz-Villanueva et al., 2014). The increased hydraulic pressure can also cause a bridge to be damaged and eventually destroyed (De Cicco et al., 2018). Historically, the potential hazards associated with LW led to wood removal from streams (Wohl, 2014). Nevertheless, in recent years, a shift in river restoration practices has seen the reintroduction of LW, recognizing its ecological benefits and contributions to river morphology (Grabowski et al., 2019; Roni et al., 2015).

Understanding the dynamics of large wood in rivers is critical (Iroumé et al., 2014; Merten et al., 2010). Laboratory studies, such as those by Braudrick et al. (1997) and Braudrick and Grant (2001), pioneered in describing wood dynamics and how it moves in rivers, describing the different transport regimes (i.e., uncongested, semicongested, and congested), highlighting how LW can flow independently in small clusters, or as a dense mass resembling a floating "carpet." Their experiments demonstrated that flow conditions, wood piece dimensions, and input rates govern transitions between these regimes. Although these transport regimes were initially established for floating LW, wood can also be moved by dragging or sliding on the channel bed (D. Ravazzolo et al., 2017). As a result, flows where wood makes up the majority of the solid portion and where the wood floats and drags have been defined as hypercongested wood flows (Ruiz-Villanueva et al., 2019).

Additionally, the experimental study by Ghaffarian et al. (2018) showed how the dimensions and geometry of floating wood influence transient motion under flow conditions. The transient motion is the adjusting phase of the wood piece's motion when hydrological conditions change. Their findings indicated that particle geometry, such as aspect ratio and the presence of root wads, significantly affects drag forces and mobility. While their experiments were conducted in controlled flume conditions, they underscored the importance of wood dimensions in shaping transport behavior, complementing insights from natural river systems. When monitoring wood during a flood, different techniques can be used (Ruiz-Villanueva et al., 2024). Traditional tagging methods, including infield numbered tags and/or Radio-Frequency Identification (RFID) tags, have limitations in spatial and temporal scale (MacVicar et al., 2009). However, recent technological advancements, such as video-based monitoring and machine learning techniques, present promising methodologies for more comprehensive and specific wood transport analyses (Aarnink, Beucler, et al., 2025; Ghaffarian et al., 2020, 2021). These techniques have been applied to videos from single cameras installed in a fixed location with a limited view of the river channel, usually oblique or perpendicular to the flow. Only a few attempts have been made to track the movement of wood over longer reaches. One of the first studies was presented by Ravazzolo et al. (2015), who used RFIDs and GPS sensors to track the displacement and trajectories of LW in a river in Italy. Another study was carried out in Poland during a 20-year flood in a wide mountain river introducing wood pieces with radio transmitters that were tracked during and after the flood (Wyżga et al., 2017). More recently, Spreitzer et al. (2024) tested inertial measurement units (IMUs) installed in prototype Smartwood pieces (wood cylinders without branches or roots) and introduced them into three rivers in Switzerland. The results of the experiments provided quantitative data on LW movement dynamics. However, the information was challenging to interpret. Groundbreaking experiments, such as those by Ghaffarian et al. (2018), Braudrick et al. (1997), and Braudrick and Grant (2001), and field tracking (Rayazzolo et al., 2015: Spreitzer et al., 2024: Wyżga et al., 2017) have greatly enhanced our understanding of wood transport in controlled conditions. However, these works did not provide insights into the relationship between the wood motion and the flow, were not performed under high flow conditions, and were limited to artificially introduced man-made wood pieces. Therefore, monitoring and characterizing wood movement during floods remains limited, and it is challenging due to technical difficulties and a lack of monitoring stations.

In this study, we combined Uncrewed Aerial Vehicles (UAVs) and Convolutional Neural Networks (CNN) (Lecun et al., 2015; van Lieshout et al., 2020) specifically trained to detect LW, to monitor wood transport during a flood. Our goals were to (a) overcome the limitations of traditional tagging and fixed-camera methods by capturing real-time LW trajectories, velocities, rotations, and orientations over a river section; (b) analyze the interaction between wood transport dynamics and detailed flow field characteristics derived from Large-Scale Particle Image Velocimetry (LSPIV); and (c) quantify the influence of wood piece dimensions on transport behavior at unprecedented spatial and temporal resolution. The observation of wood transport and mobility during floods remains scarce and a challenging task due to the unpredictable character of floods and wood transport. Experimental floods released from dam reservoirs for restoration purposes provide a unique opportunity to do so, as the time and location of the flood are set. This is the case of the Spöl River in the Swiss Alps, where such experimental floods are released annually (Consoli et al., 2022, 2023; Robinson et al., 2023), and since 2018, a group of scientists have been

AARNINK ET AL. 2 of 21



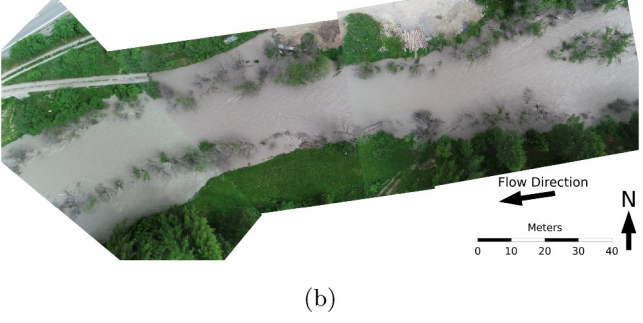


Figure 1. (a) Location of the Spöl River and the study section (in red) within the National Park shaded in gray (modified from Scheurer & Molinari, 2003) and (b) the georectified views of the three drones during flight.

monitoring LW dynamics by combining different methods (i.e., tagging, monitoring with cameras and visual counting). In this study, we present an experiment performed with three UAVs that were flown simultaneously during the rising limb of an experimental flood in 2023. By simultaneously deploying three UAVs during the flood's rising limb, and combining flow field mapping with wood tracking, we provide novel insights into the mechanics of instream wood movement that were previously unattainable.

2. Study Site and Methods

2.1. Spöl River

The study site for this research was located along the lower Spöl River, close to the village of Zernez (Canton Graübunden, Switzerland). The Spöl River is a tributary of the Inn River, with a drainage area of 286 km², which ranges from 2,316 to 1,480 m.a.s.l in elevation. The river is regulated by two dams constructed in the 1960s. The largest of the two, the Punta del Gall, is situated on the border with Italy, and the lower dam, the Ova Spin, is around 5 km upstream from the Inn River. For an overview, see Figure 1a. The continental climate is characterized by cold winters, moderate summer temperatures, and an annual rainfall of around 1,000 mm, with the peak observed in summer (based on the data from the station located in Susch (46.754883/10.083011 at 1,416 m above sea level; MeteoSwiss WIGOS-ID station 0-756-0-SUS; reference period 1991-2020). Details on the river's catchment are shown in Table 1. To mitigate the ecological impacts of the dams and the flow regulation, controlled experimental floods have been released from the two dams on the River Spöl almost every year since 2000. Despite its flow regime not being natural, its location crossing the Swiss National Park results in minimal human intervention in its wood regime. Wood is supplied to the river, naturally, mostly by bank erosion, mass movements, and snow avalanches. No wood was artificially added to the river before or during the experimental flood. Therefore, the instream wood present during the event originated from natural recruitment processes in the catchment over the past years. While the experimental floods are controlled in terms of discharge, the amount and distribution of wood available for mobilization remain uncontrolled variables.

The floods have been extensively studied to assess their effectiveness in restoring riverine processes and ecosystem integrity. Robinson and Uehlinger (2003) highlighted that experimental floods play a crucial role in mimicking natural hydrological variability, improving habitat conditions for

Table 1Characteristics of the Spöl River Catchment and the Studied Reach, the Lower Spöl (Robinson et al., 2004; Scheurer & Molinari, 2003; Uehlinger et al., 2003)

Spöl parameters	Entire spöl river	Lower spöl (studied reach)
Outlet Elevation	1,480 m a.s.l.	1,480 m a.s.l.
Max Elevation	2315 m a.s.l.	1,620 m a.s.l.
Length of the main stream	28 km	5.7 km
Average Catchment Slope	3.0%	2.5%
Drainage Area	$433 \ km^2$	$50 \ km^2$
Annual Mean Discharge at Outlet	$1.8 \ m^3/s$	$1.8 \ m^3/s$
Latitude Outlet	46.69°	46.69°
Longitude Outlet	10.09°	10.09°

AARNINK ET AL. 3 of 21





Figure 2. All wood trajectory lines and cross sections taken before and after the flood. As a background image, a snapshot of video 4 was used. The figure is displayed in a grid created locally in meters.

aquatic organisms, and flushing fine sediments from the riverbed. Their work emphasized the importance of long-term monitoring in adaptive management strategies. Mürle et al. (2003) documented how the floods reshaped river morphology, scoured accumulated sediments, and prevented excessive vegetation development on gravel bars, thereby maintaining channel complexity. Robinson et al. (2018) further demonstrated that these managed high flows led to significant ecological improvements, including reductions in periphyton biomass, increased macroinvertebrate diversity, and enhanced fish spawning success over nearly two decades of implementation. Finally, Consoli et al. (2022) provided new insights into how tributary inputs influence the ecological and geomorphological responses to experimental floods, showing that tributaries play a critical role in restoring sediment dynamics and ecosystem resilience in regulated river systems. In recent years, the wood regime (both wood storage and wood transport) of the Spöl River has been monitored mostly based on before and after floods surveys, with one prior study showing wood counts during the floods (Finch et al., 2025; Pellegrini et al., 2022; Ruiz-Villanueva et al., 2022).

The released flood in the Spöl river lasted for around 10–22 hr, and the discharge ranged between 25 and 40 m³/s (see Table S2 in Supporting Information S1). We monitored the experimental flood released on 15 June 2023. This flood had a total duration of 18 hr, with a peak discharge of 25 m³/s. The increase in discharge rose slowly, starting at 16:30 (Swiss local time), reaching the peak at 10:30, sustained for 4 hr, until it slowly fell between 14:30 and 22:30 (see Figure 4).

Because of its predictable (artificial) flood regime and its minimal human interference, the Spöl River presents a unique setting for studying LW dynamics. The specific area observed by UAVs was selected based on a combination of practical constraints (e.g., UAV access) and morphological interest. From a geomorphological perspective, river bends are particularly relevant for studying wood transport, as they introduce spatial heterogeneity in flow dynamics such as lateral shifts in velocity, turbulence, and secondary currents across the channel width and depth (Innocenti et al., 2023). Therefore, the river stretch between WGS84 Y-coordinates 2804017 and 2804195 is located right after a bend, resulting in the thalweg being on the right side of the river in the upper part of the observed area, after which it curves to the left of the river channel. Close to the area, a convenient UAV control position was located at (2804214,1175322). Situated 4.2 km downstream from the Ova Spin dam and 1.6 km upstream from the confluence with the River Inn, this 200-m section of the river was monitored (as shown in Figure 1b). During the flood, across the monitored section, the river had an average width of 30 m.

2.2. Data Acquisition

2.2.1. UAV Flights During the Flood

Five UAV flights were conducted using three DJI Phantom 4 Pro drones in parallel with a 20 megapixel CMOS sensor to capture wood transport during the flood's rising limb. The hydrograph of the flood is shown in Figure 4. Based on previous flood observations, most wood transport was expected during the rising limb (Ruiz-Villanueva

AARNINK ET AL. 4 of 21

21699011, 2025, 11, Downloaded from https://agupubs.onlinelibrary.wiley.com/doi/10.1029/2024JF008193 by Schw

Figure 3. The median of the velocities as observed in the five recordings. In the figure, two shaded areas are indicated where the flow diverges. The figure is displayed in a grid created locally in meters.

et al., 2022), and flights were scheduled accordingly at 09:30, 10:00, 10:30, 11:00, and 11:30 on the day of the flood (see Figure 5). Each drone was assigned to a different section of the river, with Drone 1 monitoring the eastern section, Drone 2 covering the central section, and Drone 3 focusing on the western section (see Figure 2). Flight altitudes were 70 m above terrain level, and durations ranged from 12.0 to 20.4 min (for details, see the Table S1 in Supporting Information S1). For each drone, the video footage was captured at a resolution of $3,840 \times 1,920$ pixels and a frame rate of 24 frames per second (fps), ensuring high-resolution data for the detection of a wide range of wood piece sizes. Five recording sessions were conducted, during which three drones captured a video each at the same time.

2.2.2. River Cross Sections and Water Level Monitoring

To better understand wood motion and its relation to geomorphic changes during the experimental flood, six cross sections (see Figure 2) were surveyed using a Trimble Real-Time Kinematic (RTK) GPS with satellite error correction provided by a nearby Swiss base station. At six locations along the observed river reach, each section followed a line between 2 marked points that were placed high enough not to be submerged by the flood. Topographical points were taken along these lines before and after the flood and used to assess morphological changes during the experimental flood. Morphological changes were analyzed by comparing these cross-sections, revealing areas of incision or erosion (i.e., lowering of channel bed elevation) and aggradation (i.e., the rise of channel bed elevation). These features were further related to wood transport observations.

Additionally, a ruler was attached to a partially submerged tree to monitor the water levels during the flood event. The ruler's elevation was acquired using the RTK GPS, and water level measurements were recorded at 30-s intervals via a time-lapse camera installed nearby. The water level during the flood was measured with a

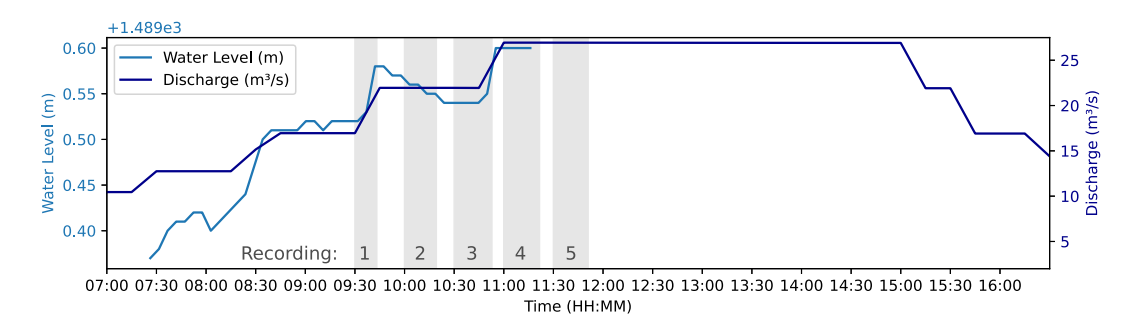


Figure 4. Water level in meters and flood discharge in m^3 /s estimated at cross-section 4. The gray bars represent the time at which the five different recordings were done. The light blue Y-axis represents the water level elevation above mean sea level.

AARNINK ET AL. 5 of 21

centimeter accuracy. This setup allowed for continuous monitoring of water levels throughout the UAV flights, with the recorded levels shown in Figure 4.

2.2.3. Ground Control Points (GCPs) and Georectification

Ground Control Points (GCPs) were necessary for ensuring the accurate georeferencing of the UAV imagery during post-processing. At least six GCPs were visible in each UAV frame, placed strategically to stand out visually and be easily detected by a custom YOLOv8 object detection algorithm (Jocher et al., 2023). The GCPs were colored in a bright orange and anchored firmly in the ground to prevent dislocation, even during high-water events. The GCPs were positioned to be visible from a drone flying approximately 60 m above the river center. Their precise locations with sub-centimeter accuracy were measured using an RTK GPS, ensuring accurate reference points for georectifying the UAV footage.

The georectification method that was implemented for this research processed all images in a certain video individually for all three vantage points. To georectify a single frame, apart from knowing the Pixel- and Geodetic Coordinates of each GCP, the internal camera parameters are required. This is necessary so that the pixels of which the Geodetic Coordinates are not known can be projected. Therefore, for each drone, an additional grid flight was conducted in manual mode using the same video recording function as was used during the experimental flood. Thereafter, the frames were cut from the video, and Agisoft Metashape was used to calculate the necessary camera parameters, including the internal camera matrix and the distortion matrix (Zhang, 2000). Using these parameters, each frame was georectified by calculating a homography matrix based on the GCPs. Homography is a mathematical transformation that enables the mapping of pixel coordinates to a real-world Cartesian coordinate system (XYZ), such as those derived from RTK GPS measurements. The georectification process was implemented using parts of the flamingo Python package (Hoonhout, 2024), which applies OpenCV for homography estimation and image transformation.

2.3. Post-Processing and Data Analysis

2.3.1. River Flow Velocity (v_r) and Convergence-Divergence

We employed Large-Scale Particle Image Velocimetry (LSPIV) using the Fudaa-LSPIV software (Coz et al., 2014) to calculate surface flow velocity from the georectified drone videos at 24 fps. This method is based on tracking the movement of surface features between successive frames using cross-correlation of image subsections to derive velocity fields. The software calculates the surface flow velocity in meters per second by analyzing how these patterns shift between frames. This method has been largely used in river monitoring and has recently been tested with the use of drones (Bodart et al., 2024; Fairley et al., 2022). We processed the video data from each of the five runs to generate velocity vectors across the river's surface at different times. Each run provided a spatial flow velocity map, with vectors indicating the flow's direction and magnitude at different locations. Due to errors in the LSPIV software, estimated velocities in certain areas of some videos were excessively high and inaccurate, whilst overall, the flow velocity was underestimated. This affected the overall average. Therefore, from the five different recordings, the median of the five estimates (one for each of the recordings) for each coordinate was used to create a more representative velocity map, which is shown in Figure 3.

Additionally, we characterized areas of converging and diverging flow by visually identifying velocity vectors in different regions. These patterns were mapped as shaded areas in the velocity field, as shown in Figure 3. The converging flow was manually identified where velocity vectors directed toward a common point indicated compression of flow lines, while the diverging flow was mapped where velocity vectors spread apart.

2.4. Wood Tracking and Dynamics

Video footage from the UAVs was processed by extracting frames at a rate of 4 fps to allow consistent tracking. An existing CNN (Aarnink, Beucler, et al., 2025) was adapted to detect instream wood from the video frames. 72 images were cropped from the UAV videos, and all pieces of wood were labeled. The 72 labeled images were combined with a pre-existing data set of 354 labeled images, enhancing the model's detection accuracy. The model architecture is based on the YOLOv8 framework (Jocher et al., 2023) and was specifically fine-tuned, using a split of data of 90% for training and 10% for validation, for detecting wood in complex environments such as mountain rivers. When the CNN detects a piece of wood, it draws a bounding box which envelopes the wood

AARNINK ET AL. 6 of 21

piece in that specific frame. The CNN ran on all frames at 24 fps, with a sensitivity threshold of 5%, meaning even detections with a low confidence score were considered for further analysis. As the output also consisted of false detections, they were then automatically filtered using the DeepSORT object tracking algorithm, discarding any detections that did not follow a consistent trajectory. This approach, while different from traditional particle tracking tools such as Trackpy or the Crocker-Grier algorithm, follows a similar goal of reconstructing object trajectories, albeit optimized for the spatial scale and visual characteristics of LW in fluvial settings. To associate individual wood detections across video frames and reconstruct their trajectories, we used the DeepSORT algorithm (Wojke et al., 2017). DeepSORT is a real-time multi-object tracking algorithm that extends the SORT algorithm by incorporating appearance features extracted through a deep convolutional neural network. It enables tracking in the presence of occlusions, missed detections, or overlapping objects, which we encountered in UAV footage due to the canopy cover and turbulent water. Each detected bounding box from the CNN was assigned an initial ID. DeepSORT matched detections across subsequent frames by combining motion prediction from a Kalman filter and appearance embeddings from a pre-trained deep network. This process helped filter out false positives by requiring temporal consistency, and allowed the assignment of a unique track ID to each piece of wood, even when reappearing after short occlusions. The DeepSORT implementation significantly reduced noise and enabled the construction of continuous wood trajectories, which were later used to compute velocities, rotation, and orientation.

Each piece was assigned an ID number and tracked throughout the observed area. The 24 fps data was reduced to 4 fps to decrease computational demand. Not all paths were perfectly analyzed because, on the one hand, the algorithm is not 100% accurate, and on the other hand, the canopy obscured the view. Therefore, in some cases, detection gaps of 0.5 s or more were still prevalent in the data. These larger gaps were not used for further velocity and angle/rotation measurements. The data set consists of a total of 560 pieces of LW that were each detected an average of 64 times (35,786 detections in total). This results in a refined set of trajectories with an average of 64 detections per piece of wood.

2.4.1. Wood Characteristics

The characteristics of wood, including length, diameter, and volume, were defined and calculated based on bounding box dimensions, pixel segmentation, and geometric assumptions.

Large wood criteria Pieces of wood are considered large wood with a diameter of at least 10 cm and a length of 1 m (Wohl et al., 2010). For the main analyses of this research, we considered both small and large wood, as we observed that a non-insignificant 35% of all tracked wood was small wood in terms of size. For some analyses we specifically state that only large wood was considered.

Wood length (L_w) The length of each piece of wood was estimated based on the bounding boxes and homographies. As the exact location of each of the corners of the bounding boxes (BBox) was known after the orientation was detected, the length was calculated as a straight line from corner to corner. The database consists of multiple length measurements as each piece was detected multiple times. The length was determined as the median of the multiple detections for each piece.

Wood diameter (D_w) The diameter was calculated by segmenting the wood pixels within the BBox. A convolutional semantic segmentation network (YOLOv8; Jocher et al., 2023) was trained on 444 labeled images, with 50 images used for validation. This network was then applied to classify pixels in all of the detected bounding boxes. As the size of each pixel is known, the total amount of segmented pixels was converted into wood surface area. Dividing this area by the length of the diagonal of the bounding box provided an estimate of the wood diameter. This calculation was done for each detection, resulting in multiple diameter measurements per piece ID. For final diameter calculation, the median of all calculated diameters was used.

Wood volume (V_w) Assuming a cylindrical shape, the volume of each piece of wood was calculated using the estimated diameter and length:

$$V_w = \frac{\pi D^2 L}{4}$$

where D is the diameter and L is the length of the wood piece.

AARNINK ET AL. 7 of 21

2.4.2. Wood Dynamics

Wood dynamics were defined by analyzing changes in individual pieces' spatial position, orientation, and velocity over time, using consecutive detections and flow field comparisons.

Wood velocity (v_w) Wood velocities were calculated for individual pieces with a detection gap of less than 1 s by dividing the distance between consecutive detections by the time gap.

Wood orientation (O_w) As a wood piece spans diagonally across its bounding box in one of two ways, the orientation was categorized as either top-left to bottom-right ("tlbr") or top-right to bottom-left ("trbl"). An edge detection algorithm was created to detect in which of the two directions the most edges were prevalent. After determining the orientation of the piece of wood within the frame, it could be compared to the stream flow direction as analyzed in Section 2.3.1.

 $Wood\ rotation\ (\phi_w)$ The rotation of a piece of wood between two frames is calculated using the spatial orientation within the bounding box across consecutive frames. For each bounding box, the angle between the coordinates of the corners is computed using the arctangent function, which measures the direction of the piece relative to the horizontal axis. To determine the rotation angle between two consecutive frames, the angle from the first frame is compared to that of the second frame, and the absolute difference between the two is taken.

2.5. Statistical Analyses

We employed a combination of normality testing, non-parametric correlation analysis, and trend visualization techniques to investigate the relationships between wood characteristics and their dynamics. These methods were selected to account for the non-Gaussian distribution of the data and potential non-linear relationships between variables

2.5.1. Normality Testing: Shapiro-Wilk Test

We applied the Shapiro-Wilk test to determine whether the dependent variables, such as wood piece velocity and rotation, followed a normal distribution (Shapiro & Wilk, 1965). This test evaluates the null hypothesis that a given data set is normally distributed. A p-value below 0.05 indicates a significant deviation from normality, meaning that parametric methods (e.g., Pearson correlation, linear regression) may not be appropriate.

2.5.2. Correlation Analysis: Spearman's Rank Correlation

If a non-normal nature was found in the data, we used Spearman's rank correlation (Spearman, 1904) coefficient (ρ) to quantify the correlation between variables. Unlike the Pearson correlation, the Spearman correlation ranks the data. It assesses whether an increase in one variable is associated with an increase or decrease in another without assuming a linear relationship.

2.5.3. Trend Visualization: Locally Weighted Scatterplot Smoothing (LOWESS)

To visualize non-linear relationships between wood properties (e.g., length, diameter, volume) and movement dynamics metrics (e.g., velocity, rotation), we applied LOWESS (Locally Weighted Scatterplot Smoothing) (Cleveland, 1979). This method fits a smooth curve to the data by performing weighted local regressions instead of assuming a fixed functional form (such as a straight line in ordinary least squares regression). We set the smoothing parameter to 0.3, balancing local sensitivity with overall trend representation.

2.5.4. Heteroscedasticity Testing: White Test and Breusch-Pagan Test

Heteroscedasticity is the presence of non-constant variance in residuals. This was tested using the White test (White, 1980) and the Breusch-Pagan test (Breusch & Pagan, 1979). These tests were used to determine whether the variance of the residuals depends on the independent variable. The White test is a general test that captures nonlinear and interaction effects in heteroscedasticity, while the Breusch-Pagan test assumes a linear relationship between the variance and independent variables. A *p*-value below 0.05 in either test suggests that heteroscedasticity is present.

AARNINK ET AL. 8 of 21

Table 2
Total Amount of Observed Large, Long, Thick and Small Wood in 5332.75 s
(88.90 min) of Video

Wood class	Number	Length (m)	Diameter (m)	Total volume (m^3)
Large	105	>1	>0.1	3.79
Long	42	>1	≤0.1	0.30
Thick	108	≤1	>0.1	0.82
Small	305	≤1	≤0.1	0.92
Total	560			5.93

2.5.5. Multiple Quantile Regression Analysis

When heteroscedasticity is present, we applied quantile regression (Koenker & Bassett, 1978) to model the relationships between wood properties and movement dynamics. Unlike standard regression methods, quantile regression estimates conditional quantiles of the response variable, allowing us to examine how predictor variables affect different portions of the distribution. We performed quantile regressions at the 25th, 50th (median), and 75th percentiles, showing the influence of independent variables change across lower, median, and higher rotation values.

2.5.6. Kernel Density Estimation (KDE)

Kernel Density Estimation (KDE) was used to analyze the distribution of LW orientations and rotations under different flow conditions. KDE is a non-

parametric way to estimate the probability density function of a variable, allowing for a smooth representation of its distribution without assuming any specific underlying form (Silverman, 1986). This method was suitable for the data set, where piece orientations and rotations showed continuous variation rather than discrete clustering. KDE plots were generated using a Gaussian kernel to highlight differences in behavior between converging and diverging flow zones.

3. Results

3.1. Acquisition Times and Volumes

The total duration of the experimental flood was 17 hr and 45 min. Based on the released discharge from the dam, the hydrograph at the observed area was estimated (see Figure 4). Until the water level tracking camera failed at 11.20, the water level was continuously monitored. During the rising limb of the experimental flood, a total of 1 hr, 28 min, and 52.75 s of footage was recorded along a stretch of approximately 200 m (see Supporting Information S1). Throughout the recordings, a total of 3.8 m³ of large wood was observed to be transported (Table 2). As shown in Table 2, the wood was categorized into four size classes: Large, Long, Thick, and Small. Small wood was the most frequently observed, with 305 pieces, while Large wood had the highest total volume, followed by Small and Thick wood. Information on the duration of the drone surveys is given in Table S1 in Supporting Information S1.

3.2. Wood Trajectories and Flow Field

In total, 35,786 detections of wood pieces have been made. Trajectories were constructed with an average amount of detections of 64 for all of the 560 observed pieces (see Table 2). The pieces of wood generally followed the preferential flow path of the river, which was separated by islands and barriers along the observed section. The flow field and the wood trajectories were analyzed separately, after which converging flow was shown to converge wood transport, and in areas of diverging flow, LW became less condensed. Figure 2 illustrates the detected trajectories of floating wood during the experimental flood event. The figure also shows the six cross-sections, labeled 1 through 6.

The velocity flow field, including surface flow velocities in the X and Y directions, is shown in Figure 3, which displays the median velocities from all five runs for each grid point. The color gradient and arrow vectors indicate the velocity and direction of the flow at various points across the river section. The analysis reveals that for 4 out of 6 sections, the highest flow velocities, reaching up to 6 m/s, are concentrated in the center of the channel, with lower velocities observed near the riverbanks. These flow patterns reflect the river's hydraulic conditions during the flood event, with faster velocities corresponding to areas of higher water depth and lower velocities near the banks due to frictional forces.

In correspondence with the water level drop shown in Figure 4, the LSPIV analysis shows a drop in average flow velocity between recording 2 and recording 3. Furthermore, the analysis showed that velocity changes were not uniform across the river: regions with higher baseline velocities experienced larger proportional increases during the flood peak, while slower-flowing regions exhibited smaller increases or even decreases (see Figures S1 and S2 in Supporting Information S1). Table 3 complements these insights by summarizing the average and 95th

AARNINK ET AL. 9 of 21

on Wiley Online Library for rules of use; OA articles are governed by the applicable Crea

Table 3
The Average and 95th Percentile Velocity of All the Cells in the 5 Recorded Video

Recording number	Average velocity (m/s)	95th percentile velocity (m/s)	Observed wood transported (m^3)
1	1.14	3.14	0.50
2	1.23	3.50	1.34
3	1.13	3.50	0.94
4	1.41	4.39	1.42
5	1.37	3.94	1.56

percentile velocities for each video as well as the observed amount of large wood transport per video. The table shows that average velocities progressively increase from 1.14 m/s in recording 1 (09:30) to 1.41 m/s in recording 4 (11:00), reflecting a general rise in flow velocity during the flood event, with fluctuations. Similarly, the 95th percentile velocities reach a peak in Video 4 at 4.39 m/s, indicating the maximum flow velocities. This relationship illustrates that areas of higher flow velocity experienced relatively larger increases in velocity when the flow rate rose.

3.3. Wood Flux, Water Stage and Volumes per Section

The five recordings (1–5, of 3 drone videos per recording) were done during the rising limb of the flood. Figure 4 shows the water level as monitored and the discharge estimated at the observed site.

The wood transport observations showed the highest rates after an increase in water level (see Figure 5). This happened throughout the observed period, with notable peaks observed during the periods corresponding to Flight 2 and later in Flights 4 and 5. Inter-flight variability revealed fluctuations in wood transport, even during phases of relatively stable water levels. Figure 5 illustrates this relationship, where the blue line represents discharge changes in m³/s, and the red line shows wood transport rates in m³/h per hour on average for the recording. The red dashed line shows the amount of wood transported in intervals of 90 s and shows that the transport greatly fluctuates from close to no wood transport to fluxes of over 16 m³/hr within the same recording (recording 2). Shaded gray areas mark the recordings, highlighting the specific periods of wood transport observations.

Morphological changes observed from the analyzed cross-sections revealed large erosion and aggradation areas (see Figure 6). When we compared this with wood transport distribution patterns across the cross-sections, we observed that in some cases (Sections 2 and 6), wood was mostly transported at areas with large erosion and in other cases (Sections 4 and 5) at the interface between erosion and aggradation, but in any case in active morphological areas (i.e., areas characterized by morphological changes).

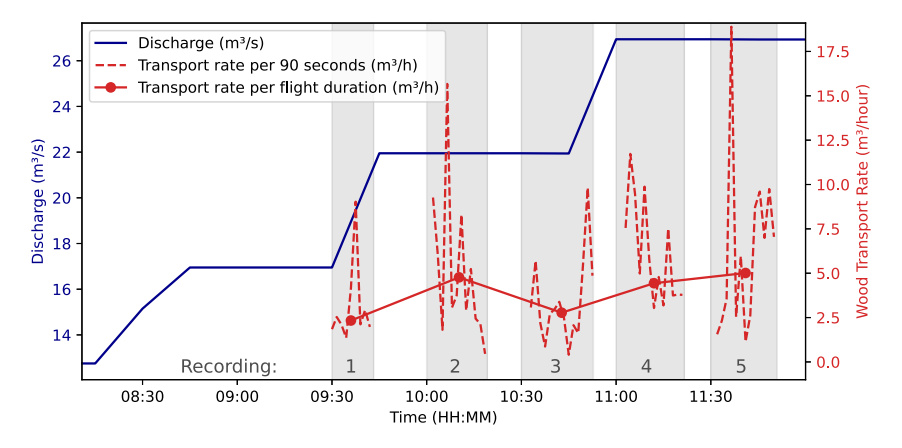


Figure 5. Discharge in m³/s and observed wood transport during the recordings. The red line represents the wood transport rate per recording, which is the observed wood transported divided by the total time of the recording. The dashed red line shows the intra-flight variability, which is the observed wood transport rate in intervals of 90 s.

AARNINK ET AL. 10 of 21

n Wiley Online Library for rules of use; OA articles are governed by the applicable Creativ

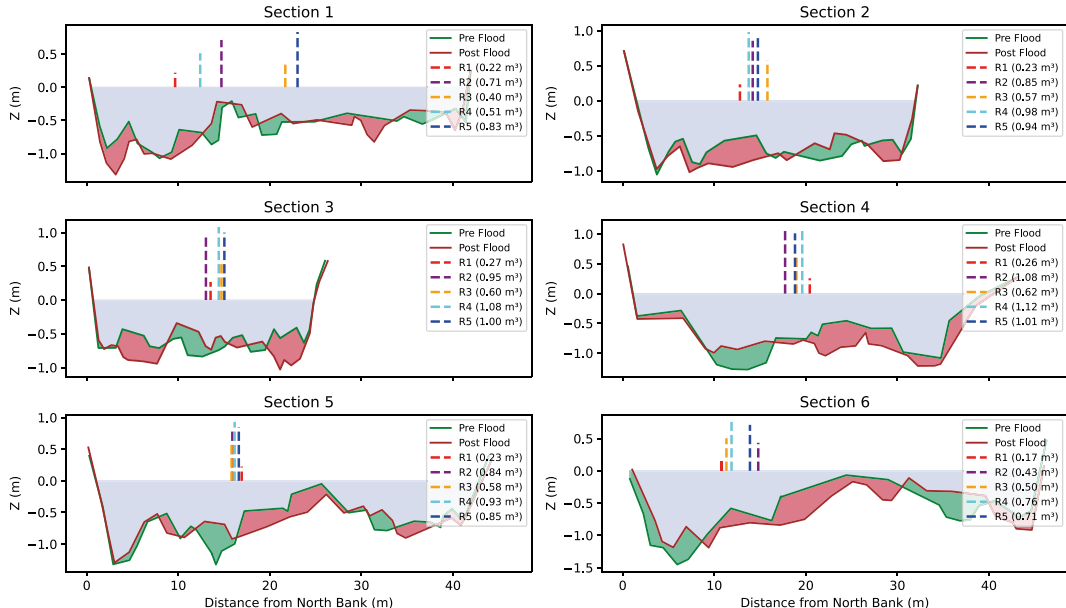


Figure 6. Sections 1 until 6 with the morphological changes and the average location of the total wood volume transport in the five different recordings. In red, degradation or erosion-dominant zones and in green, aggradation or deposition-dominant zones are indicated. The wood volume lines are drawn at the average location along the cross-section where the transport occurred. For a more detailed view, see Figures S4 and S5 in Supporting Information S1.

When looking at the average distance from the bank at which small wood (shorter than 1 m in length) and large wood (longer than 1 m in length) pass through the six different cross sections (see Table 4), we see that large and small pieces behave similarly in the section furthest upstream. Then, the trajectories diverge, with the large pieces taking a trajectory closer to the left bank of the river, which is the outer bank of the bend. In Section 2, there is a 1.5-m difference between the average distance from the bank between the two categories, after which the flow and the wood converge to a 1-m difference in Section 3. Then as flow disperses starting from Section 4, the difference again increases.

3.4. Dimensions of Transported Wood

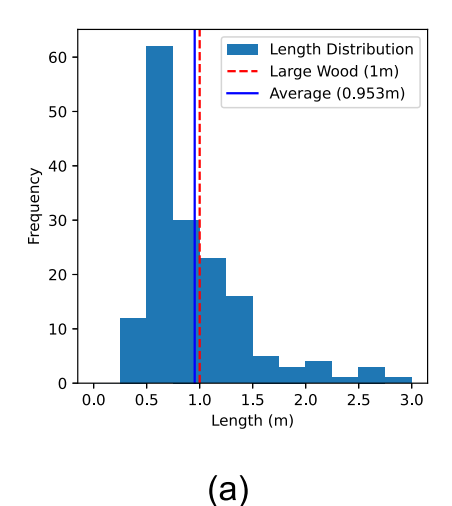
The observed wood piece dimensions (Figure 7) showed that transport during the flood event was dominated by smaller pieces in length, diameter and volume. The analysis showed that 413 out of 560 wood pieces measured less than 1 m in length, with a sharp decrease in frequency for longer pieces, and diameters were typically below 0.1 m. Despite the higher frequency of small pieces, large wood (longer than 1 m and wider than 0.1 m) pieces contributed substantially to the total volume, accounting for 65% of observed transport volume (see Table 2). Figure 7a displays the length histogram, and Figure 7b presents the diameter distribution.

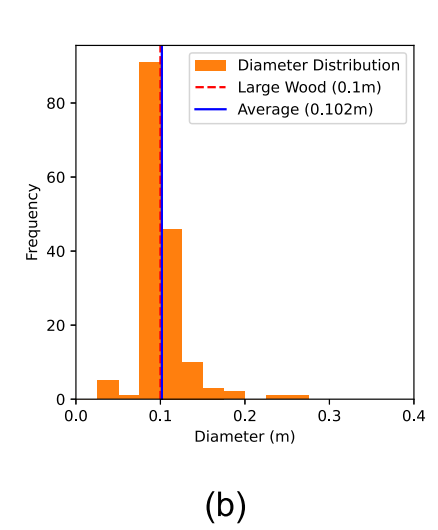
 Table 4

 Average Passing Distance From the North Bank in Meters Per Category

Average I assing Distance From the North Bank in Meters I et Category				
	Small wood (<1 m in length) (m)	Large wood (>1 m in length) (m)		
Section 1	22.69	23.08		
Section 2	13.51	14.99		
Section 3	14.20	15.23		
Section 4	18.29	18.95		
Section 5	15.81	16.77		
Section 6	11.38	14.30		

AARNINK ET AL. 11 of 21





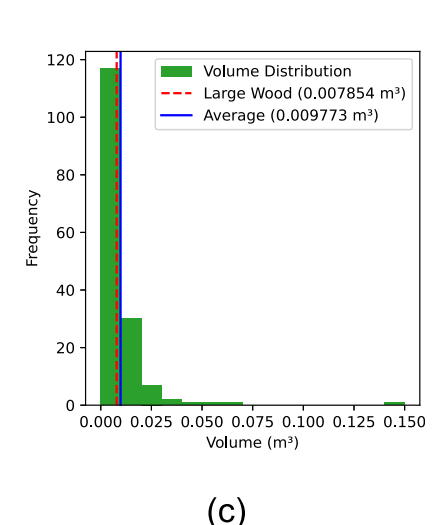


Figure 7. Histograms of lengths (a) diameters (b) and volumes (c) of all observed pieces of wood. The red dashed line indicates the minimum values for a piece to satisfy the large wood criteria. The blue line is the average of all observed pieces of wood.

When looking at the top 20 largest wood pieces observed during the flood event (Figure 8a), the data showed their contribution to the total volume transported was substantial at 35%. Notably, two pieces that exceeded 0.25 m³ in volume underscored their large contribution. One of these, piece 2.38, recorded in video 2, measured 2.72 m in length and 42 cm in diameter, while piece 5.28 from video 5 was 5.38 m long with a 28 cm diameter. Aside from these two largest pieces, the volumes of individual pieces decreased more gradually. Figure 8a presents a Pareto graph showing all recorded pieces. Figure 8b shows the volume contribution of the 20 largest pieces, and in Figure 8c, the two largest detected pieces of wood are highlighted.

3.4.1. Wood Velocity

The distribution of wood piece velocities (Figure 9) revealed that 81% of wood velocity observations were between 2.5 and 4.5 m/s. This range represents the typical velocity observed for pieces in the data set. The distribution shows a slight positive skew, with fewer pieces reaching higher velocities, up to around 6–7 m/s. These higher velocities are rare, indicating that while wood pieces generally moved at moderate velocities, certain conditions in wood characteristics and the flow field allowed for occasional faster movement. Figure 9 shows the histogram of the typical and extreme velocity ranges of wood pieces during the observed period and also shows the LSPIV velocity histogram. If the LSPIV velocities are accurately estimated, the wood pieces seem to travel through the fastest sections of the river. However, further analyses have shown that the LSPIV software underestimates the flow velocity.

When looking at only pieces of wood that fulfill the large wood requirements (i.e., >1 m long and >10 cm diameter), the relationship between the wood piece velocity and the physical dimensions of the pieces showed some weak trends (see Figure 10). According to the Spearman Correlation, wood piece length shows a weak but significant positive association with wood piece velocity over the whole range of lengths (see Figure 10a). The LOWESS trendline, however, shows more local trends, which start with an increase in wood piece velocity when piece length increases up until a length of approximately 2.3 m. It shows that the wood piece velocity decreases from 3.7 m/s for pieces of 2.3 m in length to 3.0 m/s for pieces of 4.4 m in length. When considering the diameter of the piece, Figure 10b shows a different but still significant trend, although weaker. It shows how the wood piece velocity of pieces between 0.1 and 0.24 m decreases (from approximately 3.8 m/s to 3.3 m/s) with increasing diameter. Above a diameter of 0.24 m, the velocity does not seem to differ much.

The relationship between the ratio of wood piece length to diameter and piece velocity (Figure 11) shows a positive but weak correlation, with a change in the local trend around a length-diameter ratio of 16. The wood piece velocity trendline ranges from approximately 3.4 m/s to 3.9 m/s and sees its steepest increase between the length-diameters ratios of 12 and 16.

AARNINK ET AL. 12 of 21

21699011, 2025, 11, Downloaded from https://agupubs.onlinelibrary.wiley.com/doi/10.1029/2024F008193 by Schweizerische Akademie Der, Wiley Online Library on [10/11/2025]. See the Terms and Conditions (https://onlinelibrary.wiley.com/doi/10.1029/2024F008193 by Schweizerische Akademie Der, Wiley Online Library on [10/11/2025]. See the Terms and Conditions (https://onlinelibrary.wiley.com/doi/10.1029/2024F008193 by Schweizerische Akademie Der, Wiley Online Library on [10/11/2025]. See the Terms and Conditions (https://onlinelibrary.wiley.com/doi/10.1029/2024F008193 by Schweizerische Akademie Der, Wiley Online Library on [10/11/2025]. See the Terms and Conditions (https://onlinelibrary.wiley.com/doi/10.1029/2024F008193 by Schweizerische Akademie Der, Wiley Online Library on [10/11/2025]. See the Terms and Conditions (https://onlinelibrary.wiley.com/doi/10.1029/2024F008193 by Schweizerische Akademie Der, Wiley Online Library on [10/11/2025]. See the Terms and Conditions (https://onlinelibrary.wiley.com/doi/10.1029/2024F008193 by Schweizerische Akademie Der, Wiley Online Library on [10/11/2025]. See the Terms and Conditions (https://onlinelibrary.wiley.com/doi/10.1029/2024F008193 by Schweizerische Akademie Der, Wiley Online Library on [10/11/2025]. See the Terms and Conditions (https://onlinelibrary.wiley.com/doi/10.1029/2024F008193 by Schweizerische Akademie Der, Wiley Online Library on [10/11/2025]. See the Terms and Conditions (https://onlinelibrary.wiley.com/doi/10.1029/2024F008193 by Schweizerische Akademie Der, Wiley Online Library on [10/11/2025]. See the Terms and Conditions (https://onlinelibrary.wiley.com/doi/10.1029/2024F008193 by Schweizerische Akademie Der, Wiley Online Library on [10/11/2025]. See the Terms and Conditions (https://onlinelibrary.wiley.com/doi/10.1029/2024F008193 by Schweizerische Akademie Der, Wiley Online Library on [10/11/2025]. See the Terms and Conditions (https://onlinelibrary.wiley.com/doi/10.1029/2024F00819 by Schweizerische Akademie Der, Wiley Online Bernary on [10/11/2025]. See t

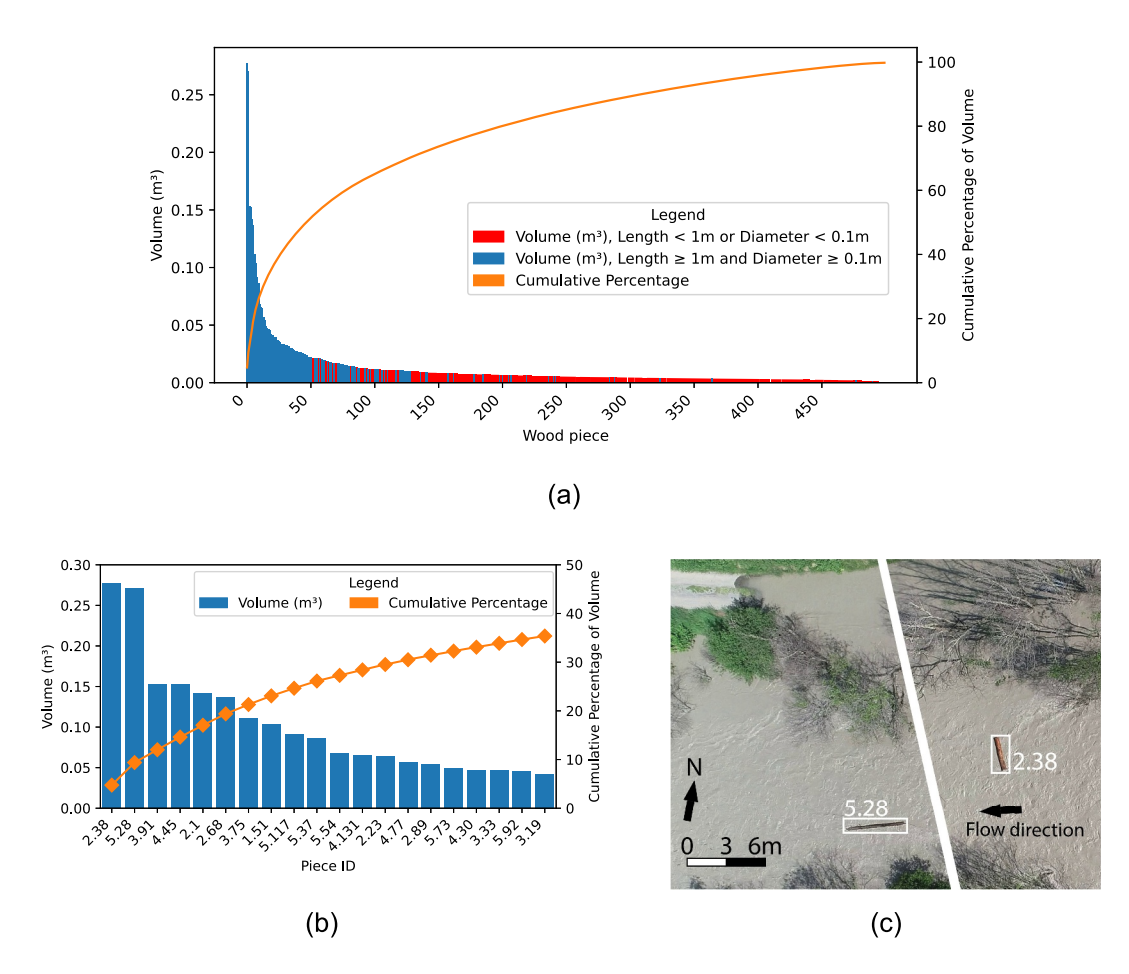


Figure 8. (a) Pareto graph showing the 20 largest pieces observed, indicating a clear difference between the two largest recorded pieces of wood and the rest of the observations. (b) Pareto Graph of the volume of each piece of wood for the 500 largest pieces. The orange line represents the cumulative volume. Pieces in red do not fulfill the large wood criteria. (c) The two largest pieces in the data set are shown in the inset picture. Piece number 2.38 (recording 2, number 38, length: 2.72 m, diameter: 42 cm) on the left and number 5.28 (recording 5, number 28, length: 5.38 m, diameter: 28 cm) on the right.

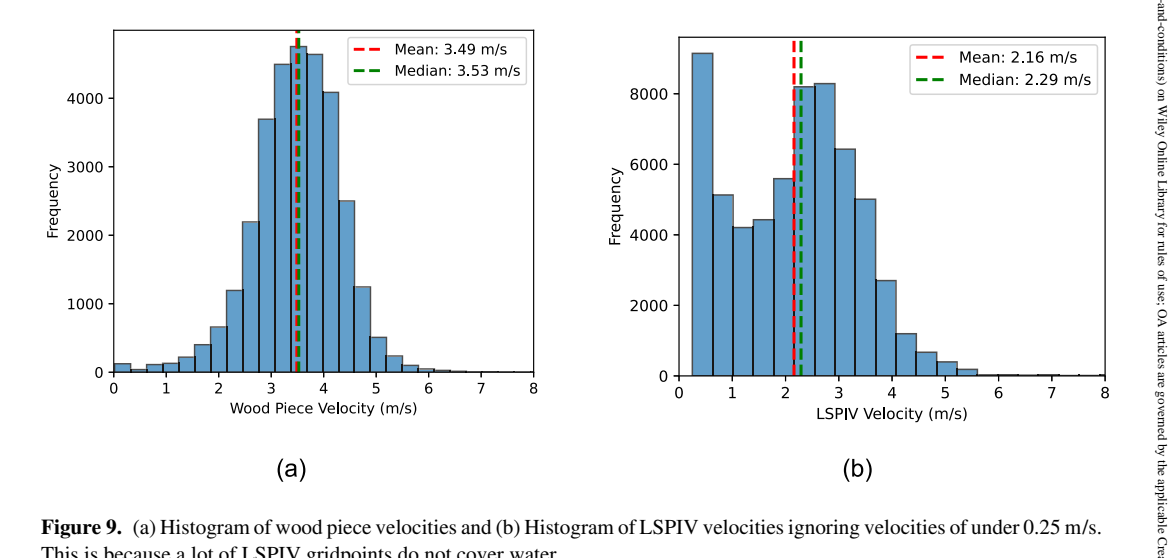


Figure 9. (a) Histogram of wood piece velocities and (b) Histogram of LSPIV velocities ignoring velocities of under 0.25 m/s. This is because a lot of LSPIV gridpoints do not cover water.

AARNINK ET AL. 13 of 21

21699011, 2025, 11, Downloaded from https://agupubs.onlinelibrary.wiley.com/doi/10.1029/2024JF008193 by Schweir

Akademie Der, Wiley Online Library on [10/11/2025].

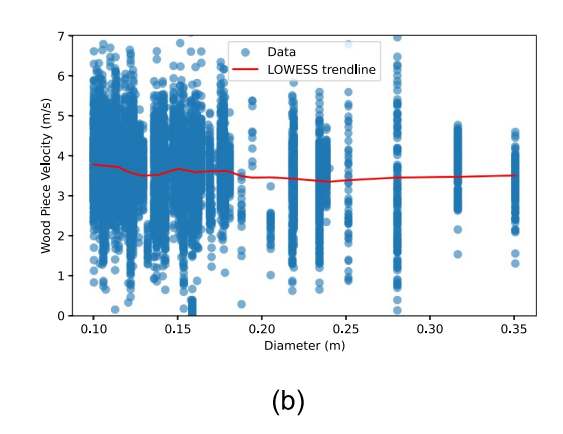


Figure 10. Wood piece velocity versus piece length (a, Spearman trend: $\rho = 0.026$, P = 0.008) and piece diameter (b, Spearman trend: $\rho = -0.113$, P = 0.000). Due to the non-linear nature of the dependent variable (Shapiro-Wilk test: W = 0.981, P-value = 0.000), a Spearman correlation was calculated, and in red, a LOWESS trendline is shown. Only pieces that fulfill the large wood requirements have been taken into account.

3.5. Wood Orientation

The analysis shows that wood pieces in diverging areas (as marked in Figure 3) display a broader distribution of angles, indicating less alignment and greater variability in orientation. In contrast, pieces in converging flow areas exhibit a stronger alignment with the flow direction, with a higher density of wood piece angles below 20° compared to pieces in diverging areas. These findings are visualized in Figure 12a, where the Kernel Density Estimation (KDE) plot highlights the differences in wood piece angle distributions between the two flow patterns. The Mann-Whitney U test confirms that these differences are statistically significant. Additionally, when looking at the angles in general, the analysis showed that the majority of wood pieces flow at small angles relative to the flow direction, with the highest frequency occurring at angles between 0 and 20°. Figure 12a shows the distribution of wood piece angles with respect to the flow direction for large wood detections. Approximately 40% of the pieces had an angle of less than 20°, indicating that wood in converging flow is more parallel than perpendicular to the flow. As the angle increased, the frequency of wood pieces flowing at higher angles decreased significantly, with the lowest occurrence between 80 and 90°. When comparing the orientations of the detected pieces of wood to the flow velocity, Figure 12b shows a weak negative overall correlation. This suggests that as flow velocity increased, the angle at which the pieces were oriented concerning the flow direction tended to decrease. The local trendline, however, indicates that this correlation is not generally applicable. Wood piece angles seem to increase with increasing wood piece velocity for angles below 20°. Furthermore, we see that higher wood piece angles have a narrower range of velocities.

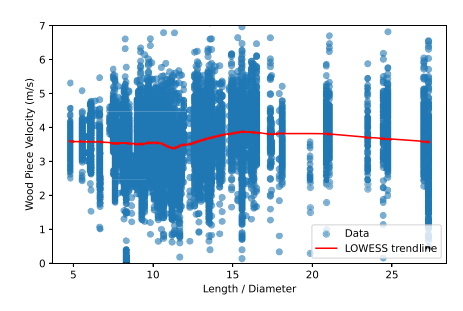


Figure 11. Wood piece velocity versus the ratio between length and diameter. Due to the non-linear nature of the dependent variable (Shapiro-Wilk test: W = 0.981, P-value = 0.000), and in red, a LOWESS trendline is shown (Spearman trend: $\rho = 0.108$, P = 0.000). Only pieces that fulfill the large wood requirements have been taken into account.

3.6. Wood Rotation

The results of the rotation analysis (Figure 13a) show that in diverging flow areas (as marked in Figure 3), wood pieces exhibited a slightly broader distribution of rotation angles, indicating a slightly greater variability in their movement. On the other hand, pieces of wood in converging flow areas showed a slightly higher density at slower rotation speeds and a slightly lower density at higher rotation speeds than pieces in diverging areas. This suggests that pieces of wood in converging regions were slightly more stable and experienced less rotational movement due to the flow dynamics. These patterns are shown in Figure 13a, which shows the Kernel Density Estimation (KDE) plot of wood piece rotation for both flow patterns; however, the differences were small. Although the Mann-Whitney U test confirms that the rotation distributions in converging and diverging areas were statistically significantly different.

When looking at the relation between the flow velocity and the rotation of the pieces of wood, we see a gradual increase in rotation when the velocity increases. However, the trend does not seem to hold at the highest velocities. Figure 13b

AARNINK ET AL. 14 of 21

21699011, 2025, 11, Downloaded from https://agupubs.onlinelibrary.wiley.com/doi/10.1029/2024JF008193 by Schweizerische

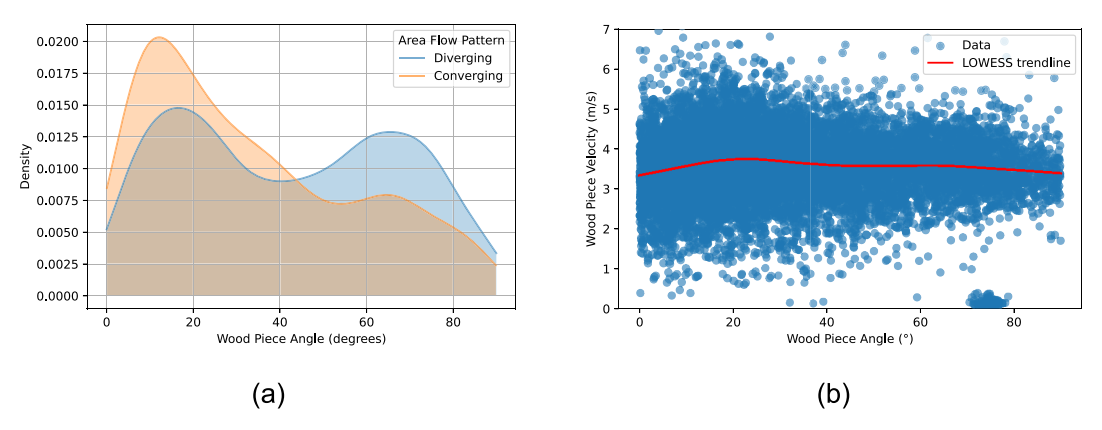


Figure 12. (a) Kernel Density Estimation (KDE) plot of wood piece angles with respect to flow direction when comparing converging to diverging flow areas. (b) Scatter plot of wood piece orientation with respect to piece velocity, with a LOWESS local trendline (Spearman trend: $\rho = -0.023$, P = 0.024). Only pieces that fulfill the large wood requirements have been taken into account.

presents a KDE plot that examines the relationship between piece rotation and flow velocity derived from the LSPIV data. In the figure, the KDE plot of rotation versus velocity reveals a dense concentration of data at lower rotation angles, indicating that most pieces experienced minimal rotation across the range of velocities, with 76% of rotation observations below 4°/0.25s.

For the relationships between rotation and wood characteristics, we tested whether heteroscedasticity was present between the variables in all three cases (Rotation vs. Length, Rotation vs. Diameter, and Rotation vs. Volume). In all cases, the White test and the Bresch-Pagan test had p-values close to zero, and heteroscedasticity was assumed. Then, we ran multiple quantile regression for q = 0.25, q = 0.5 and q = 0.75, of which the results are shown in Figure 14. The analysis revealed a consistent negative correlation between wood piece rotation and the three primary piece dimensions: length, diameter, and volume. These relationships were statistically significant and illustrated by the downward-sloping trend lines for all quantiles across the subfigures. In terms of length, as shown in Figure 14a, longer wood pieces tended to exhibit less rotation, with pieces above 3 m in length consistently showing lower rotation values. This pattern suggests that larger, more stable wood pieces were less prone to rotational motion, according to the observations in this study. Similarly, Figure 14b demonstrates that pieces with greater diameters tended to rotate less than thinner pieces, indicating a negative correlation between rotation and piece diameter. Lastly, Figure 14c shows the same trend for increased piece volume. Larger-volume pieces of wood experienced less rotational movement compared to smaller pieces. The analyses indicated that the effect was most pronounced for faster-rotating pieces as shown by the 0.75 quantile regression lines.

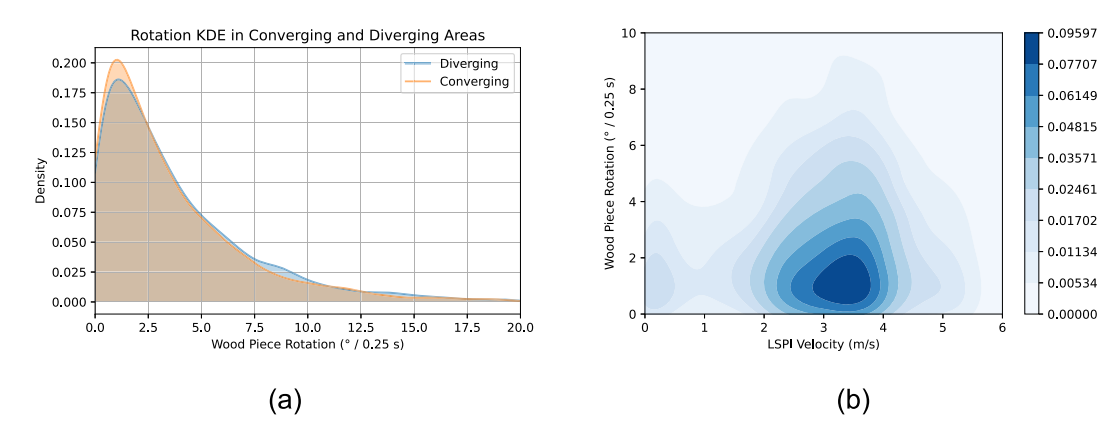


Figure 13. (a) Kernel Density Estimation (KDE) plot of wood piece rotation when comparing converging to diverging flow areas and (b) wood piece rotation versus stream flow velocity. Only pieces that fulfill the large wood requirements have been taken into account.

AARNINK ET AL. 15 of 21

21699011, 2025, 11, Downloaded from https://agupubs.onlinelibrary.wiley.com/doi/10.1029/2024JF008193 by Schwei

Akademie Der, Wiley Online Library on [10/11/2025].

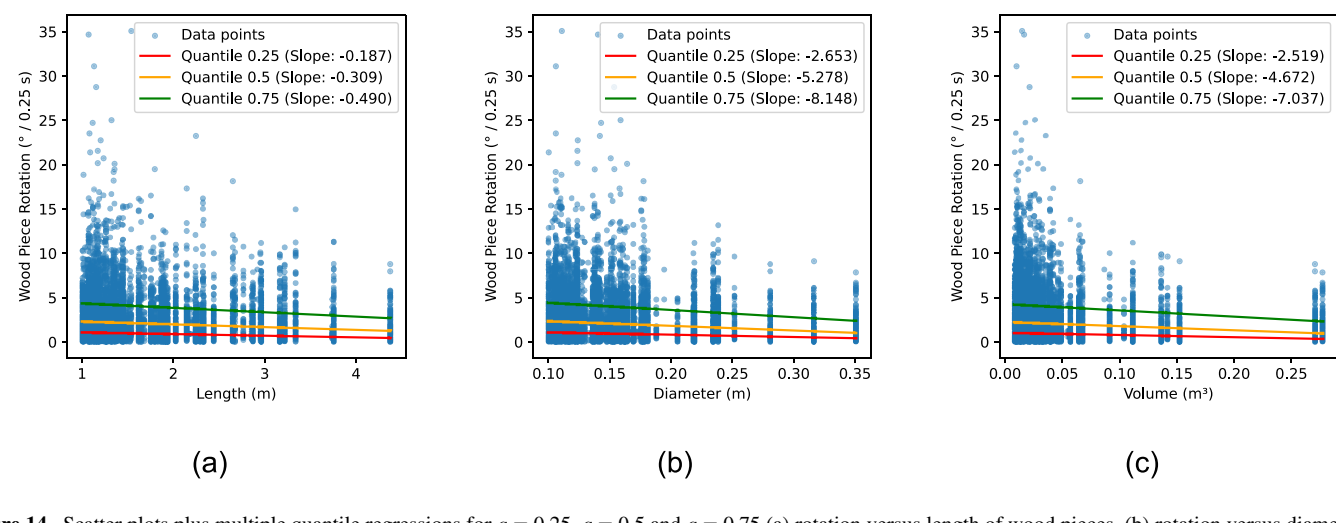


Figure 14. Scatter plots plus multiple quantile regressions for q = 0.25, q = 0.5 and q = 0.75 (a) rotation versus length of wood pieces, (b) rotation versus diameter of wood pieces and (c) rotation versus volume of wood pieces. Only pieces that fulfill the large wood requirements have been taken into account.

4. Discussion

This study quantified uncongested large wood (LW) transport dynamics during an experimental flood, utilizing high-resolution video and machine learning-based monitoring in the Spöl River in the Swiss Alps. The size and detail of the real-world data set generated were unprecedented. Our findings highlight how the flow patterns and wood piece dimensions affect the mobility and rotation of large wood, providing new insights into the dynamics of instream wood transport. While most studies on wood transport dynamics have been conducted in controlled flumes (Braudrick et al., 1997; Ghaffarian et al., 2018), or used man-made artificially reintroduced wood (Spreitzer et al., 2024; Wyżga et al., 2017), this is the first study to track wood movement during a flood event where wood pieces were individually tracked, their dimensions estimated, and their velocity and orientation determined on a detailed 4 fps framerate.

The analysis of LW trajectories showed that wood transport was primarily concentrated within the river's high-flow velocity paths. We do not see constantly increasing flow velocities throughout the observed period. The decrease in flow velocity (both on average and the 95th percentile, see Table 3 and Figure 3) and water level (Figure 5) from recording 2 to 3 suggests some local erosion and/or aggradation patterns influencing the hydraulics during the flood. Our wood mobility findings align with the transport mode described by Braudrick et al. (1997) and Braudrick and Grant (2001), who identified the effects of flow conditions and wood geometry on transport dynamics. While their work observed how wood pieces tended to align with flow direction under varying channel conditions, our study demonstrated similar behavior during natural floods, showing that piece alignment reduces rotational dynamics, particularly for larger pieces, in high-velocity flow paths.

Our study also found that large pieces of instream wood contribute importantly to the overall wood volume transported. The two largest pieces alone accounted for approximately 7% of the total transported volume, underlining the disproportionate contribution of a few large pieces to the total wood fluxes. While small wood was more frequent, with 455 out of 560 pieces not fulfilling the large wood requirements, it accounted for a much smaller proportion of the total volume (35%), as observed in other studies (e.g., Galia et al., 2018). This disproportionality is also observed in sediment transport in mountain rivers, where larger-grained sediment accounts for a disproportionately large share of the total transport, and the bedload transport stage (during which coarser sediments start moving) requires a certain discharge threshold (Lenzi et al., 2006).

Large wood (defined as pieces of wood longer than 1 m in length and thicker than 0.1 m in diameter) comprised 65% of the observed wood volume, despite smaller pieces outnumbering them by a factor of 5. These findings suggest that, while smaller pieces of wood are prevalent, large pieces play a more substantial role in terms of volume and potential geomorphic impact on the river system. Although wood in the other three categories does not fulfill the traditional large wood (LW) definition, it still accounts for nearly 40% of the total transported wood. Since our method allows for fully automated detection, it may be beneficial in these cases to be less strict in excluding smaller samples so we can capture a more complete picture of instream wood transport. When looking

AARNINK ET AL. 16 of 21

at the intra-flight variability of wood transport (see Figure 5), the two large peaks in recordings 2 and 5 can be explained by the transport of the two largest pieces that, because of their size of over 0.25 m^3 and the duration of the 90-s intervals, results in a transport of 10 m^3 /hour alone.

Morphological changes and the distribution of wood volume transport across six sections of the river channel during the flood event revealed localized variations without a consistent trend in lateral wood transport distribution along the cross-section (see Figure 6). On the other hand, when looking at the distance from the north bank at which small and large pieces were transported (see Table 4) we saw that large pieces tended to follow the outer bend over the middle section of the recorded area. This finding can be linked by the characteristic response distance found by Ghaffarian et al. (2018). They found that larger pieces have a longer response distance. The bend at the end of the recorded area does not seem to behave in the same way as the other bends. The outer bend there looks to be less confined than the left bank in Section 3. This can explain why we don't see the reversal of the larger pieces following the outer bend in this area. Recordings 2, 4, and 5 captured higher average transport volumes, suggesting that increased water levels drove significant wood movement. Even though this general trend was also observed in previous studies (Ruiz-Villanueva et al., 2016, 2022), our data gives a detailed view of wood transport in relation to the discharge stages released by the dam. The discharge released by the dam did not increase linearly but in steps due to the operation of the dam, which differs from a natural flood hydrograph, where a smoother increase may be expected. Our data suggests that the increase in wood transport had a slight delay with respect to the increasing discharge.

A comparison with the study performed by Spreitzer et al. (2024) highlights complementary methodological advancements. While they used IMU-tagged pieces of wood (i.e., SmartWood) to capture intra-piece dynamics such as yaw, roll, and pitch, our study utilized observed wood dynamics over broader spatial and temporal scales. Whereas their method allows for highly detailed and accurate data regarding the dynamic movement of wood, they could only perform relatively limited observations due to the costly nature of their research. On the other hand, although less accurate, our drone-based study observed overlapping transport characteristics (from rotational dynamics to the role of piece shape and size) on a larger scale. They found that wood pieces diverging from the center of the stream increased in rotational velocity. We did, on the other hand, not find a relation between velocity (as a proxy for in-stream position) and angular velocity. Furthermore, they captured localized interactions, such as impacts with riverbanks and infrastructure, whereas our approach provided a large enough database to perform statistical analyses on wood transport dynamics patterns, including flow alignment and transport velocity relationships. Both methodologies faced unique challenges (sensor drift and discontinuous IMU data vs. submerged wood detection and UAV data processing), indicating the trade-offs in studying complex fluvial systems.

Our UAV-based monitoring approach captured real-time transport processes, revealing how flow velocity and piece geometry directly influence wood movement. We observed that flow conditions and wood size played a role in transport dynamics, with pieces often aligning with flow direction during transport, in agreement with other studies (Braudrick & Grant, 2001). A comparison with Ghaffarian et al. (2018) highlights the interplay between experimental and field-scale approaches to studying LW dynamics. They investigated the transient motion of idealized floating particles in controlled flume conditions, exploring metrics such as particle characteristic response distance and the influence of particle geometry on mobility. They found that longer pieces of wood take longer to adjust to the flow velocity fully, due to their higher mass. Our study expands on these principles in a natural flood context, observing how wood piece dimensions influence wood piece velocity. We found that the diameter of the piece had a weak negative relation to the piece velocity, especially for diameters between 0.1 and 0.25 m, in this river and during the studied flood event. The comparison is complicated, as their theoretical analyses of drag forces only considered steady flow, whereas, in the natural environment we observed, steady flow is rare. The influence of physical wood characteristics on wood piece velocity showed a complex trend (Figure 11). According to the analysis, the general trend (although weak) showed that longer, thinner pieces exhibited higher velocities. Considering that the response distance is determined by mass (inertia) (Ghaffarian et al., 2018), longer, thinner pieces of wood have a relatively low mass when compared to its drag forces (as the diameter is squared when calculating mass) and, therefore, have a shorter response length, exhibiting higher velocities in our measurements. This would also explain why the diameter was observed to have a larger effect on the piece velocity in Figure 10.

Flow patterns influenced wood piece orientation, with converging flow areas promoting alignment with the flow direction. Pieces in these regions exhibited smaller angles relative to the flow, reducing variability compared to

AARNINK ET AL. 17 of 21

diverging zones. This finding underscores the role of flow convergence in stabilizing wood piece trajectories, aligning with theoretical frameworks that link flow dynamics to particle orientation as described by Braudrick and Grant (2001). They showed that pieces of wood tend to rotate into a flow-parallel orientation due to velocity gradients acting on different ends of the piece. Our results reveal a complex relationship between wood piece rotation and flow velocity. While piece rotation generally increased with flow velocity, it plateaued and even decreased at the highest velocities, possibly due to diminished back-propagation of disturbances in high flow conditions. The influence of wood dimensions on rotation further indicated that larger pieces of wood, particularly those with greater diameter, exhibited less rotational movement. This inverse relationship, more pronounced with diameter than length, may be attributed to the increased inertia from larger diameters, which dampens rotational response.

While this study provides valuable insights into LW dynamics during floods, several limitations should be acknowledged. First, our observations were restricted to a relatively short river reach (200 m) and a limited time window, primarily due to logistical constraints associated with drone operations, such as battery life. These spatial and temporal limitations may not capture the full variability of wood transport processes across different flood stages or river morphologies. In future works, it would be interesting to extend the observation area further upstream to include the vegetated island that appears in the upstream part in Figure 2. This would allow us to analyze the diverging and converging patterns of wood transport more deeply. However, the lack of suitable locations to install GCPs and the limitations of the area covered by each drone prevented us from doing this. Previous observations in the river indicated that the majority of wood transport occurred during the rising limb of the hydrograph, and the tracking study was planned accordingly. This pattern is also consistent with findings from sediment transport studies (Malutta et al., 2020). However, because the entire flood event was not continuously monitored due to logistical constraints, our ability to fully characterize transport dynamics throughout all phases of the hydrograph was limited. A more detailed analysis of wood transport across the complete flood, including recession, is therefore explored in further work. Additionally, flow characterization relied on Large-Scale Particle Image Velocimetry (LSPIV) applied to drone imagery. Although LSPIV has been validated for surface velocity measurements using drone data (Fairley et al., 2022; Lewis et al., 2018), it inherently captures only surface flow patterns and may not fully represent the complex three-dimensional structure of the flow field, relatively turbulent and turbid in our case, leading to potential inaccuracies in velocity estimations. Incorporating complementary methods, such as acoustic Doppler current profilers (ADCP) or computational fluid dynamics (CFD) modeling, could improve the characterization of subsurface flow conditions (Tauro et al., 2016). Furthermore, while this study focused on wood movement patterns, a more comprehensive understanding of transport mechanisms requires direct computation of hydrodynamic forces acting on wood pieces, including drag, lift, and torque, which are critical for accurately modeling wood behavior during floods (Shields & Alonso, 2012). Moreover, our observations were limited to an uncongested transport regime, where wood pieces moved independently without significant interactions (Braudrick et al., 1997). Tracking floods that exhibit other transport regimes, such as congested or hypercongested conditions (Ruiz-Villanueva et al., 2019), would provide a more comprehensive understanding of large wood dynamics in rivers during floods. Capturing these different regimes could reveal critical transitions in transport behavior and their implications for flood risk and riverine ecosystem processes.

5. Conclusions

This study explored large wood (LW) transport dynamics during an experimental flood in the Spöl River (Swiss Alps), using high-resolution UAV monitoring and machine learning techniques. By tracking around 36,000 individual wood detections across a 200-m river section, we showed patterns in wood mobility, velocity, rotation, and alignment with the flow.

Our findings highlight the significance of wood piece dimensions in transport behavior, with longer, thinner pieces moving faster due to reduced drag, while thicker pieces experienced slower velocities due to higher resistance. Flow convergence consistently promoted piece alignment, reducing variability in orientation and stabilizing trajectories. Larger pieces of wood were found to rotate less than smaller ones, with their higher inertia decreasing rotational movement, especially in high-velocity flows. These dynamics underscore the complex interplay between flow characteristics and wood geometry.

The study's novel methodology bridges the gap between laboratory experiments and real-world conditions, validating and expanding upon controlled studies. Furthermore, comparisons with recent advancements, such as

AARNINK ET AL. 18 of 21



Journal of Geophysical Research: Earth Surface

10.1029/2024JF008193

the use of IMU-tagged wood pieces, and flume experiments, illustrate how large natural data sets can be used to draw parallels between theoretical and natural wood movement.

Future research should aim to expand the temporal and spatial scales of these observations to better understand long-term trends and regional variations in LW transport dynamics. Also, a less strict requirement for large wood dimensions can be considered in automatic detections, including small wood to compute wood fluxes. Integrating UAV-based monitoring with other technologies, such as sensor-equipped pieces of wood or multi-scale hydrodynamic modeling, will further advance our understanding of the interactions between large wood, flow, and river morphology.

Data Availability Statement

The code is available from Aarnink (2025) and the data is available from Aarnink, Fornari, et al. (2025).

Acknowledgments References

This work has been supported by the Swiss

Lausanne and Bern (Switzerland), with the

collaboration of the Swiss National Park

Special thanks to Flavio Calvo and Margot

comments from Dr. Nakul S. Deshpande,

Sirdey for their help in GCP detection

MacVicar, Prof. Stuart Lane and Prof.

Pascale Biron on an early version of the

manuscript, who helped us significantly

improve the paper. Open access publishing

facilitated by Université de Lausanne, as

part of the Wiley - Université de Lausanne

agreement via the Consortium Of Swiss

Academic Libraries.

using triangulation. We thank the

Dr. John T. Kemper, Prof. Bruce

National Science Foundation project

PCEFP2186963 and the Universities of

Aarnink, J. (2025). Code for processing Spoel River data. Retrieved from https://github.com/janbertoo/process_spoel_data

Aarnink, J., Beucler, T., Vuaridel, M., & Ruiz-Villanueva, V. (2025). Automatic detection of floating instream large wood in videos using deep learning. Earth Surface Dynamics, 13(1), 167–189. https://doi.org/10.5194/esurf-13-167-2025

Aarnink, J., Fornari, A., Rouge, F., & Ruiz-Villenueva, V. (2025). Dataset for wood piece tracking used in the study. Zenodo. https://doi.org/10.5281/zenodo.14245569

Andreoli, A., Comiti, F., & Lenzi, M. A. (2007). Characteristics, distribution and geomorphic role of large woody debris in a mountain stream of the Chilean Andes. *Earth Surface Processes and Landforms*, 32(11), 1675–1692. https://doi.org/10.1002/esp.1593

Bodart, G., Le Coz, J., Jodeau, M., & Hauet, A. (2024). Quantifying and reducing the operator effect in LSPIV discharge measurements. *Water Resources Research*, 60(2), e2023WR034740. https://doi.org/10.1029/2023WR034740

Braudrick, C. A., & Grant, G. E. (2001). Transport and deposition of large woody debris in streams: A flume experiment. *Geomorphology*, 41(4), 263–283. https://doi.org/10.1016/s0169-555x(01)00058-7

Braudrick, C. A., Grant, G. E., Ishikawa, Y., & Ikeda, H. (1997). Dynamics of wood transport in streams: A flume experiment. Earth Surface Processes and Landforms, 22(7), 669–683. https://doi.org/10.1002/(SICI)1096-9837(199707)22:7<669::AID-ESP740>3.0.CO;2-L

Breusch, T. S., & Pagan, A. R. (1979). A simple test for heteroscedasticity and random coefficient variation. *Econometrica: Journal of the Econometric Society*, 47(5), 1287–1294. https://doi.org/10.2307/1911963

Chen, X., Wei, X., Scherer, R., & Hogan, D. (2008). Effects of large woody debris on surface structure and aquatic habitat in forested streams, southern interior British Columbia, Canada. *River Research and Applications*, 24(6), 862–875. https://doi.org/10.1002/rra.1105

Cleveland, W. S. (1979). Robust locally weighted regression and smoothing scatterplots. *Journal of the American Statistical Association*, 74(368), 829–836. https://doi.org/10.2307/2286407

Consoli, G., Haller, R. M., Doering, M., Hashemi, S., & Robinson, C. T. (2022). Tributary effects on the ecological responses of a regulated river to experimental floods. *Journal of Environmental Management*, 303, 114122. https://doi.org/10.1016/j.jenyman.2021.114122

Consoli, G., Siebers, A. R., Bruder, A., & Robinson, C. T. (2023). Long-term reconstruction of energy fluxes in an alpine river: Effects of flow

regulation and restoration. *River Research and Applications*, 39(9), 1783–1794. https://doi.org/10.1002/rra.4189
Coz, J. L., Jodeau, M., Hauet, A., Marchand, B., & Boursicaud, R. L. (2014). Image-based velocity and discharge measurements in field and

laboratory river engineering studies using the free FUDAA-LSPIV software. River Flow, 1961–1967. https://doi.org/10.1201/b17133-262

De Cicco, P. N., Paris, E., Ruiz-Villanueva, V., Solari, L., & Stoffel, M. (2018). In-channel wood-related hazards at bridges: A review. River Research and Applications, 34(7), 617–628. https://doi.org/10.1002/rra.3300

Fairley, I., Williamson, B. J., McIlvenny, J., King, N., Masters, I., Lewis, M., et al. (2022). Drone-based large-scale particle image velocimetry applied to tidal stream energy resource assessment. *Renewable Energy*, 196, 839–855. https://doi.org/10.1016/j.renene.2022.07.030

Finch, B. D., Gibaja del Hoyo, J., Aarnink, J. L., O'Callaghan, M., & Ruiz-Villanueva, V. (2025). Monitoring the large wood regime in a partially regulated alpine river following several experimental floods. (in press).

Galia, T., Ruiz-Villanueva, V., Tichavský, R., Šilhán, K., Horáček, M., & Stoffel, M. (2018). Characteristics and abundance of large and small instream wood in a Carpathian mixed-forest headwater basin. Forest Ecology and Management, 424(May), 468–482. https://doi.org/10.1016/j. foreco.2018.05.031

Ghaffarian, H., Lemaire, P., Zhi, Z., Tougne, L., MacVicar, B., & Piégay, H. (2021). Automated quantification of floating wood pieces in rivers from video monitoring: A new software tool and validation. *Earth Surface Dynamics*, 9(3), 519–537. https://doi.org/10.5194/esurf-2020-96

Ghaffarian, H., Lopez, D., Riviere, N., Piégay, H., & Mignot, E. (2018). Experimental study of the transient motion of floats reproducing floating wood in rivers. In E3S Web of Conferences (Vol. 40, p. 02041). https://doi.org/10.1051/e3sconf/20184002041

Ghaffarian, H., Piégay, H., Lopez, D., Rivière, N., MacVicar, B., Antonio, A., & Mignot, E. (2020). Video-monitoring of wood discharge: First inter-basin comparison and recommendations to install video cameras. *Earth Surface Processes and Landforms*, 45(10), 2219–2234. https://doi.org/10.1002/esp.4875

Grabowski, R. C., Gurnell, A. M., Burgess-Gamble, L., England, J., Holland, D., Klaar, M. J., et al. (2019). The current state of the use of large wood in river restoration and management. *Water and Environment Journal*, 33(3), 366–377. https://doi.org/10.1111/wej.12465

Gurnell, A. M., Piégay, H., Swanson, F. J., & Gregory, S. V. (2002). Large wood and fluvial processes. Freshwater Biology, 47(4), 601–619. https://doi.org/10.1046/j.1365-2427.2002.00916.x

Hassan, M. A., Bird, S., Reid, D., & Hogan, D. (2016). Simulated wood budgets in two mountain streams. Geomorphology, 259, 119–133. https://doi.org/10.1016/j.geomorph.2016.02.010

Hoonhout, B. (2024). Flamingo. Retrieved from https://github.com/openearth/flamingo

Innocenti, L., Bladé, E., Sanz-Ramos, M., Ruiz-Villanueva, V., Solari, L., & Aberle, J. (2023). Two-dimensional numerical modeling of large wood transport in bended channels considering secondary current effects. Water Resources Research, 59(12), e2022WR034363. https://doi.org/10.1029/2022WR034363

AARNINK ET AL. 19 of 21



Journal of Geophysical Research: Earth Surface

- 10.1029/2024JF008193
- Iroumé, A., Mao, L., Ulloa, H., Ruz, C., & Andreoli, A. (2014). Large wood volume and longitudinal distribution in channel segments draining catchments with different land use, Chile. *Open Journal of Modern Hydrology*, 4(2), 57–66. https://doi.org/10.4236/ojmh.2014.42005
- Jocher, G., Qiu, J., & Chaurasia, A. (2023). YOLO by ultralytics. Retrieved from https://github.com/ultralytics/ultralytics/
- Koenker, R., & Bassett, G. J. (1978). Regression quantiles. Econometrica: Journal of the Econometric Society, 46(1), 33–50. https://doi.org/10.2307/1913643
- Lecun, Y., Bengio, Y., & Hinton, G. (2015). Deep learning. Nature, 521(7553), 436-444. https://doi.org/10.1038/nature14539
- Lenzi, M., Mao, L., & Comiti, F. (2006). Effective discharge for sediment transport in a mountain river: Computational approaches and geomorphic effectiveness. *Journal of Hydrology*, 326(1), 257–276. https://doi.org/10.1016/j.jhydrol.2005.10.031
- Lewis, Q. W., Lindroth, E. M., & Rhoads, B. L. (2018). Integrating unmanned aerial systems and LSPIV for rapid, cost-effective stream gauging. Journal of Hydrology, 560, 230–246. https://doi.org/10.1016/j.jhydrol.2018.03.008
- MacVicar, B., Piegay, H., Henderson, A., Comiti, F., Oberlin, C., & Pecorari, E. (2009). Quantifying the temporal dynamics of wood in large rivers: Field trials of wood surveying, dating, tracking, and monitoring techniques. Earth Surface Processes and Landforms, 34(15), 2031–2046. https://doi.org/10.1002/esp.1888
- Malutta, S., Kobiyama, M., Chaffe, P. L. B., & Bonumá, N. B. (2020). Hysteresis analysis to quantify and qualify the sediment dynamics: State of the art. Water Science and Technology, 81(12), 2471–2487. https://doi.org/10.2166/wst.2020.279
- May, C. L., & Gresswell, R. E. (2003). Processes and rates of sediment and wood accumulation in headwater streams of the Oregon Coast Range, USA. Earth Surface Processes and Landforms, 28(4), 409–424. https://doi.org/10.1002/esp.450
- Merten, E., Finlay, J., Johnson, L., Newman, R., Stefan, H., & Vondracek, B. (2010). Factors influencing wood mobilization in streams. Water Resources Research. 46(10). https://doi.org/10.1029/2009WR008772
- Mürle, U., Ortlepp, J., & Zahner, M. (2003). Effects of experimental flooding on riverine morphology, structure and riparian vegetation: The River Spöl, Swiss National Park, Aquatic Sciences, 65(3), 191–198. https://doi.org/10.1007/s00027-003-0665-6
- Pellegrini, G., Martini, L., Rainato, R., & Picco, L. (2022). Large wood mobilization and morphological changes in an alpine river following the release of an ordinary experimental flood from an upstream dam. Catena, 216, 106398. https://doi.org/10.1016/j.catena.2022.106398
- Platts, W. S., Armour, C. L., Booth, G. D., Bryant, M., Bufford, J. L., Cuplin, P., et al. (1987). Methods for evaluating riparian habitats with applications to management. Retrieved from https://api.semanticscholar.org/CorpusID:140148382
- Ravazzolo, D., Mao, L., Mazzorana, B., & Ruiz-Villanueva, V. (2017). Brief communication: The curious case of the large wood-laden flow event in the Pocuro stream (Chile). Natural Hazards and Earth System Sciences, 17(11), 2053–2058. https://doi.org/10.5194/nhess-17-2053-2017
- Ravazzolo, D., Mao, L., Picco, L., & Lenzi, M. (2015). Tracking log displacement during floods in the Tagliamento River using RFID and GPS tracker devices. *Geomorphology*, 228, 226–233. https://doi.org/10.1016/j.geomorph.2014.09.012
- Rickenmann, D., & Koschni, A. (2010). Sediment loads due to fluvial transport and debris flows during the 2005 flood events in Switzerland. Hydrological Processes, 24(8), 993–1007, https://doi.org/10.1002/hyp.7536
- Robinson, C. T., Consoli, G., & Ortlepp, J. (2023). Importance of artificial high flows in maintaining the ecological integrity of a regulated river. Science of the Total Environment, 882, 163569. https://doi.org/10.1016/j.scitotenv.2023.163569
- Robinson, C. T., Siebers, A. R., & Ortlepp, J. (2018). Long-term ecological responses of the River Spöl to experimental floods. Freshwater Science, 37(3), 433–447. https://doi.org/10.1086/699481
- Robinson, C. T., & Uehlinger, U. (2003). Using artificial floods for restoring river integrity. Aquatic Sciences, 65(3), 181–182. https://doi.org/10.1007/s00027-003-0002-0
- Robinson, C. T., Uehlinger, U., & Monaghan, M. T. (2004). Stream ecosystem response to multiple experimental floods from a reservoir. *River Research and Applications*, 20(4), 359–377. https://doi.org/10.1002/rra.743
- Roni, P., Beechie, T., Pess, G., & Hanson, K. (2015). Wood placement in river restoration: Fact, fiction, and future direction. Canadian Journal of Fisheries and Aquatic Sciences, 72(3), 466–478. https://doi.org/10.1139/cjfas-2014-0344
- Ruiz-Villanueva, V., Aarnink, J., Ghaffarian, H., Gibaja del Hoyo, J., Finch, B., Hortobágyi, B., et al. (2024). Current progress in quantifying and monitoring instream large wood supply and transfer in rivers. Earth Surface Processes and Landforms, 49(1), 256–276. https://doi.org/10.1002/esp.5765
- Ruiz-Villanueva, V., Aarnink, J., Gibaja, J., Finch, B., & Vuaridel, M. (2022). Integrating flow-, sediment- and instream wood-regimes during eflows in the Spöl River (Swiss Alps). In *Proceedings of the 39th IAHR World Congress(June)* (pp. 611–615). https://doi.org/10.3850/IAHR-
- Ruiz-Villanueva, V., Bodoque, J. M., Díez-Herrero, A., & Bladé, E. (2014). Large wood transport as significant influence on flood risk in a mountain village. Natural Hazards, 74(2), 967–987. https://doi.org/10.1007/s11069-014-1222-4
- Ruiz-Villanueva, V., Mazzorana, B., Bladé, E., Bürkli, L., İribarren-Anacona, P., Mao, L., et al. (2019). Characterization of wood-laden flows in rivers. Earth Surface Processes and Landforms, 44(9), 1694–1709. https://doi.org/10.1002/esp.4603
- Ruiz-Villanueva, V., Mikuś, P., Hajdukiewicz, H., & Stoffel, M. (2016). The role of flood hydrograph in the remobilization of large wood in a wide mountain river. *Journal of Hydrology*, 541, 330–343. https://doi.org/10.1016/j.jhydrol.2016.02.060
- Scheurer, T., & Molinari, P. (2003). Experimental floods in the River Spöl, Swiss National Park: Framework, objectives and design. *Aquatic Sciences*, 65(3), 183–190. https://doi.org/10.1007/s00027-003-0667-4
- Shapiro, S. S., & Wilk, M. B. (1965). An analysis of variance test for normality (complete samples). *Biometrika*, 52(3/4), 591–611. https://doi.org/10.1093/biomet/52.3-4.591
- Shields, F. D., Jr., & Alonso, C. V. (2012). Assessment of flow forces on large wood in rivers. Water Resources Research, 48(4). https://doi.org/10.1029/2011WR011547
- Silverman, B. (1986). Density estimation for statistics and data analysis. Chapman & Hall.
- Spearman, C. (1904). The proof and measurement of association between two things. American Journal of Psychology, 15(1), 72–101. https://doi.org/10.2307/1412159
- Spreitzer, G., Schalko, I., Boes, R., & Weitbrecht, V. (2024). SmartWood: Field-based analysis of large wood movement dynamics using inertial measurement units (IMUs). *Environmental Sciences Europe*, 36(1), 94. https://doi.org/10.1186/s12302-024-00916-7
- Tauro, F., Petroselli, A., & Arcangeletti, E. (2016). Assessment of drone-based surface flow observations. *Hydrological Processes*, 30(7), 1114–1130. https://doi.org/10.1002/hyp.10698
- Uehlinger, U., Kawecka, B., & Robinson, C. T. (2003). Effects of experimental floods on periphyton and stream metabolism below a high dam in the Swiss Alps (River Spöl). Aquatic Sciences, 65(3), 199–209. https://doi.org/10.1007/s00027-003-0664-7
- van Lieshout, C., van Oeveren, K., van Emmerik, T., & Postma, E. (2020). Automated River plastic monitoring using deep learning and cameras. *Earth and Space Science*, 7(8), e2019EA000960. https://doi.org/10.1029/2019EA000960
- White, H. (1980). A heteroscedasticity-consistent covariance matrix estimator and a direct test for heteroscedasticity. Econometrica: Journal of the Econometric Society, 48(4), 817–838. https://doi.org/10.2307/1912934

AARNINK ET AL. 20 of 21

- Wohl, E. (2014). A legacy of absence: Wood removal in US rivers. Progress in Physical Geography, 38(5), 637–663. https://doi.org/10.1177/0309133314548091
- Wohl, E., Cenderelli, D. A., Dwire, K. A., Ryan-Burkett, S. E., Young, M. K., & Fausch, K. D. (2010). Large in-stream wood studies: A call for common metrics. Earth Surface Processes and Landforms, 35(5), 618–625. https://doi.org/10.1002/esp.1966
- Wohl, E., Scott, D. N., & Lininger, K. B. (2018). Spatial distribution of channel and floodplain large wood in forested River corridors of the Northern rockies. Water Resources Research, 54(10), 7879–7892. https://doi.org/10.1029/2018WR022750
- Wojke, N., Bewley, A., & Paulus, D. (2017). Simple online and realtime tracking with a deep association metric. In 2017 IEEE International Conference on Image Processing (ICIP) (pp. 3645–3649). https://doi.org/10.1109/ICIP.2017.8296962
- Wyżga, B., Mikuś, P., Zawiejska, J., Ruiz-Villanueva, V., Kaczka, R. J., & Czech, W. (2017). Log transport and deposition in incised, channelized, and multithread reaches of a wide mountain river: Tracking experiment during a 20-year flood. *Geomorphology*, 279, 98–111. https://doi.org/10.1016/j.geomorph.2016.09.019
- Zhang, Z. (2000). A flexible new technique for camera calibration. *IEEE Transactions on Pattern Analysis and Machine Intelligence*, 22(11), 1330–1334. https://doi.org/10.1109/34.888718

AARNINK ET AL. 21 of 21